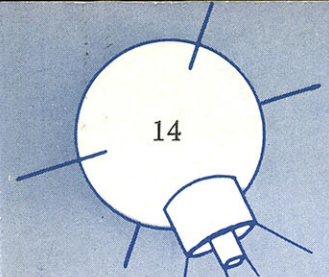

MESOMETEOROLOGY PROJECT

Department of the Geophysical Sciences
The University of Chicago

INVESTIGATION OF A SUMMER JET STREAM USING TIROS AND AEROLOGICAL DATA

by

Kozo Ninomiya

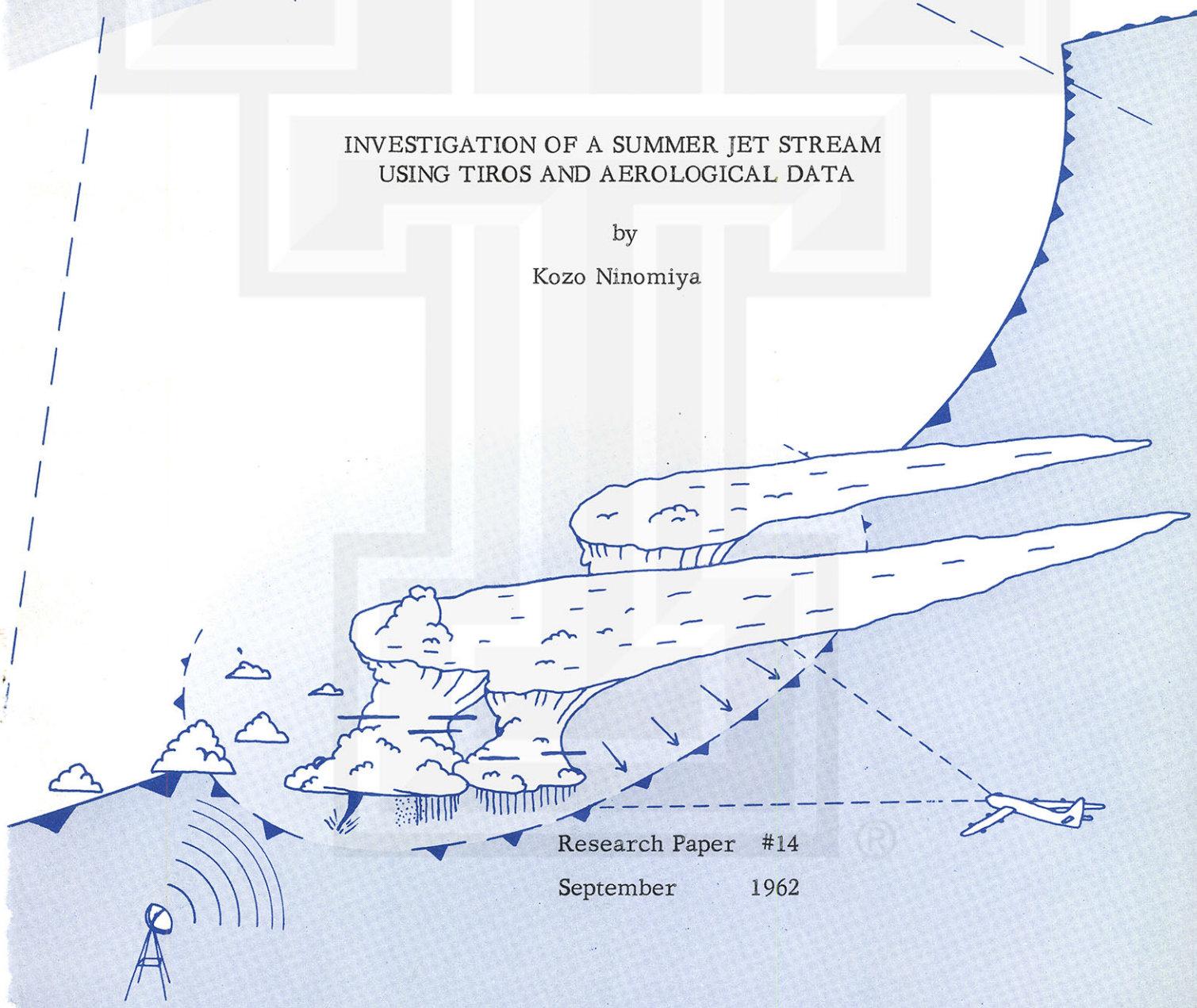

Research Paper #14

September 1962

RESEARCH PAPER # 14

MESOMETEOROLOGICAL PROJECT
Department of the Geophysical Sciences
The University of Chicago

INVESTIGATION OF A SUMMER JET STREAM USING TIROS AND AEROLOGICAL DATA

by

Kozo Ninomiya
Japan Meteorological Research Institute

The research has been supported primarily by the Japan Scientific and Technology Agency under the scholarship program and partially by the United States Weather Bureau under contract Cwb 10215 (MSL).

Table of Contents

Abstract

Precisely rectified TIROS cloud photographs are used in the analysis of the summer jet streams over the United States. The cloud distribution obtained from these photographs is compared with the divergence and vorticity field calculated from the aerological data. The situations in the vicinity of jet streams are discussed with these quantities and cloud observations.

I. Introduction

Since 1960 the TIROS series of meteorological satellites have televised back to the Earth large amounts of cloud photographs, making it possible for us to add new, useful information about the atmosphere.

In this paper the author attempts to investigate summer jet streams over the United States on September 18, 1961, using TIROS III photographs and aerological data.

During the past twenty years, many synoptic and theoretical investigations on the jet stream and related phenomena have been accomplished. The results of these investigations until 1954 were summarized in the Monograph by Riehl et al. (1954). Kochansky (1955) studied the mean cross sections along 80W for four seasons, finding that the axis of the mean-westerly wind is located along about 45N at the 12-km level in July and that in October there are two jet axes at 49N, 11 km, and 37N, 12 km. With regard to the mean tropopause, he showed that the southern edge of the polar tropopause is located at 40N, 13 km in July and 30N, 11 km in October; for the tropical tropopause its northern edge is at 14 km in July and 15 km in October. Also he pointed out the existence of a tropopause leaf over the tropopause break between the polar and tropical tropopause.

A series of new findings was made by the "Project Jet Stream", in which aircraft were used extensively. Notably, Endlich and McLean (1957) found the existence of jet-stream fronts in the upper troposphere and the fact that the wind velocity increases rapidly with height above the boundary of the jet front, reaching

the maximum between the frontal surface and the tropopause. Similar upper fronts associated with jet streams were also reported by Mohri (1957) in his analysis over the Far East.

Using smoothed wind profiles, Reiter (1957) studied the layer of maximum wind. He constructed charts of the height and the speed of maximum winds, leading him to find that the zone of lowest height of maximum wind speed is in the cyclonic side about 100 km from the jet axis.

Defant and Taba (1958) investigated tropopause change associated with a break down of zonal circulation. They showed that the hemispheric tropopause chart, in which there were two lines of tropopause breaks, polar and subtropical breaks, is very useful in the understanding of large scale atmospheric situations. Taba (1959) obtained mean horizontal and vertical wind profiles of both polar and subtropical jet streams representative of certain periods of winter.

Characteristic cloud patterns, especially the elongated ones, have been supposed to indicate the strong winds aloft. There are several investigations with regard to this phenomenon. Schaefer (1953) classified characteristic cloud types associated with jet streams as cirrus streamers, cirrocumulus, and altocumulus. He then explained the characteristic features of jet-stream clouds. Based on case studies of jet-stream clouds, Schaefer and Hubert (1955) pointed out that a jet cloud is found generally in the warm air side of a jet stream in the entrance region, and that the fine structure of the cloud is mainly due to the turbulence. They suggested the relations between turbulence, dynamical stability, and the Richardson theorem. McLean (1957) constructed vertical cross-section charts of the frequency in percent of various cloud types which are obtained in the "Jet Stream Project". It is learned that the area of maximum frequency of cirrocumulus exists between the jet front and the maximum wind level. There are two maxima of cirrus frequency; one is to the south of the jet core, and the other, which is not pronounced, is located in the vicinity of the polar tropopause. The layer above the level of the maximum is characterized by clear air.

More generally, Kuettner (1959) discussed the band structure of the atmosphere, defining "cloud streets" as a system of long rows of clouds stretching in the direction of general winds. He pointed out that the vertical change in the wind shear is usually about 10^{-7} cm^{-1} sec^{-1} for the cloud streets. He described a typical jet cloud as a cirrus shield extending to the south of a jet core with its sharp northern edge parallel

to the jet stream. As a result of photogrammetric analysis of aerial and ground photography, Conover (1960) summarized that jet clouds exist most frequently within 400 km from the jet core on the warm air side of the entrance or the neutral area, and that the northern edge of cirrus sheets are generally found about 100 km south of the jet core. He also explained that cirrus is often found on both sides of the jet stream when the jet is weak or when there are double jets.

Even before the first meteorological satellite was launched, Widger and Touort (1957) discussed the utilization of meteorological observations by satellites. They explained with the use of hypothetical data the usefulness of these observations for both meteorological research and routine work. Since the beginning of the TIROS series, a number of synoptic studies, such as those by Kruger and Fritz (1961) and by Bowley et al. (1962), were made using the cloud photographs televised from the satellites.

Fujita (1961) developed a new method of rectification of satellite cloud photographs. In principle, this method consists mainly of transformation between image and terrestrial coordinates. It is learned that this method yields a very high accuracy.

II. General Situations

In this section the meteorological situations prior to and during the analysis period are discussed briefly.

On September 14, 1961, an occluded cyclone, into which hurricane Carla had redeveloped, moved rapidly northeastward. A deep trough was induced in the upper troposphere with the cold out break which took place to the rear of the cyclone in the lower troposphere. As the cyclone moved northeastward, a cold anticyclone covered the eastern half of the United States. Another cyclone with an occluded front approached the west coast on the following day. This occluded cyclone was related to a cut-off low in the upper troposphere. These were the main meteorological systems in existence during the period of this research. There appeared another front in higher latitudes on September 16, when the meandering flow in the middle troposphere gradually changed into a zonal flow. In the upper troposphere, however, the flow still maintained its large amplitude.

The surface chart for 0000 GMT, Sept. 18, (Fig. 1) indicates the pattern of a

cold anticyclone over the southeastern United States. A cold front extends from the northwestern Atlantic to the Florida peninsula along the eastern edge of the anticyclone. To the west of the anticyclone an area of high temperature is associated with a southerly flow. An occluded front over Arizona extends westward into the Pacific while the western end of it is a weak cold front. To the north of this cold front, over the Pacific in higher latitudes, a cold anticyclone is situated. The mesoscale high-pressure area over the United States-Canadian border is characterized by rainy and overcast weather, suggesting that it would be caused by the precipitation.

The contour field on the 850-mb surface resembled the pressure field of the surface chart. The intensity of the eastern cold anticyclone indicated a marked decrease on the 850- and the 700-mb surfaces, while the intensity of the trough seen over the occluded cyclone in the west coast increased with height.

As can be seen in Fig. 2, a trough at 500 mb is located above the surface cold anticyclone. The cut-off low, which is accompanied by 50-knot winds over the west coast, is deeper than that at 700 mb. In higher latitudes flow is rather zonal with wind speed of about 40 knots.

At 300 mb both the cut-off low and the trough were deeper. A small cut-off low was found also in the eastern trough. A large pressure gradient with associated strong westerlies was seen over the northern region.

As shown in Fig. 3, the contour field at 200 mb consists mainly of two cut-off lows and three ridges; one between the cut-off lows; others over the Pacific and the Atlantic. Two axes of wind maxima exist at 200 mb. One is located along the northern edge of the subtropical highs in the upper troposphere, while the other, in the northern latitudes, is extending from the Aleutian Islands to the west coast of Canada, where the maximum wind speed reaches above 120 knots. Where the above mentioned two flows meet in front of these cut-off lows, they form typical confluence patterns. To the north of the northern flow axis the temperature field appears to be reversed. Namely, the warm areas exist over the north region where the tropopause is below 200 mb.

Above the tropopause the pressure gradient and the wind speed gradually decreased and flow became more zonal with height due to the reversed temperature gradient. At the 100-mb surface the intensity of the troughs was very weak; the flow was almost zonal, and the wind speed was less than 40 knots. With regard to the

temperature field, a warm area of about -50C was found in the north and the coldest area of about -70C in the region of the subtropical highs.

III. Distributions of Divergence and Vorticity

It is generally known that the value of the horizontal velocity divergence in cyclone-scale atmospheric motions is very small; the calculation of this quantity is sensitive to errors in observations. These errors can, sometimes, be larger than the value itself. Therefore, the calculated value must be considered as qualitative rather than quantitative.

In order to compute the divergence by the kinematic method, the coordinate system is identified with latitude and longitude. The x axis is along the latitude lines and is positive eastward. The y axis, along the longitude lines, is positive northward. Using this coordinate system, the divergence becomes

$$\nabla \cdot \mathbf{V} = \frac{\partial u}{\partial x} + \frac{\partial v}{\partial y} - \frac{v}{a} \tan \phi \quad ;$$

ϕ is the latitude, a is the Earth's radius, u and v are the west and south wind components respectively. If the order of the magnitude of the third term were considered, $\frac{v}{a}$ would be approximately 5×10^{-6} sec^{-1} for v of 30 m sec^{-1}, which was the maximum value found in the entire study, and $\tan\phi$ would be about one or smaller than one because the region of interest was to the south of 50N. Therefore, the maximum value of the third term in this study is 5×10^{-6} sec^{-1}. Since the concern in this study is with order of magnitudes of 10^{-5} sec^{-1} and higher, the third term is neglected in the computation.

Using the same system of coordinates, the vertical component of the vorticity is

$$q = \frac{\partial v}{\partial x} - \frac{\partial u}{\partial y} + \frac{u}{a} \tan \phi \quad .$$

Again the third term was neglected since the order of magnitude of the maximum value of this term was less than the order of magnitude of interest.

In order to obtain values of the wind components at grid points, isotachs and

isogons were drawn for the reported distribution of winds. Wind directions and speeds were determined at grid points from the isogon and isotach analyses; then these were converted to the values of the wind components. From these components the divergence and vorticity were computed using finite differences. The interval over which the changes in the component winds were measured was four degrees. The divergence and vorticity were computed for the 850-, 700-, 500-, 300-, 200-, and 100-mb surfaces.

On the 850-mb surface, as shown in Fig. 4, areas of convergence exist along the front near the east coast and to the northeast of the occluded cyclone on the west coast. Almost the entire region of the surface anticyclone is covered by an area of divergence. To the northwest of the anticyclone rather complex patterns, namely an area of large convergence and a narrow band of divergence, are seen over the surface mesoscale high-pressure area. The areas of divergence and convergence, enclosed by the lines of 10^{-5} sec^{-1}, are considered to be related to the lower level trough and ridge systems of easterly flow.

Although the pattern of divergence at 700 mb resembled the pattern at 850 mb, the magnitude at 700 mb was about one half the magnitude of divergence at 850 mb. At 500 mb the value of divergence was yet smaller; even the maximum value of convergence, which was associated with the cut-off low, was less than $5x10^{-6}$ sec^{-1}.

As seen in Fig. 5, which shows the distribution of divergence at 300 mb, the maximum value reaches $3x10^{-5}$ sec^{-1}. In general, the sign of the divergence is opposite to that in the lower troposphere; that is, regions of positive values are to the east of troughs and negative values to the west. Although there are no significant differences between the divergence patterns at 300 and 200 mb, the locations of the maxima and minima at 200 mb are a few hundred kilometers west of the corresponding points in the pattern at 300 mb. At 100 mb the values of divergence again become smaller than 10^{-5} sec^{-1} and the patterns are therefore considered erratic.

If a value of vertical velocity at the ground surface were assumed, the vertical velocity could be calculated by the integration of the continuity equation using calculated values of divergence at each pressure surface. However, a realistic value of the divergence in the layer between 850 mb and the ground surface is difficult to obtain without additional information, especially in mountainous regions. For this reason, the mean value of divergence was computed graphically for the layer between

the 700- and the 850-mb surface. As can be seen in the resulting pattern (Fig. 6), the maximum value is approximately 10^{-5} sec^{-1}.

The maximum value of the mean divergence in the layer between 200 mb and 300 mb was approximately twice the value shown in Fig. 6, but of opposite sign. This difference in absolute value would probably be reduced to zero if the divergence in the layer between the 850-mb and the ground surface were considered.

The correspondence between the vorticity field and the wind field was more easily determined than the correspondence of the divergence field with the wind field. In the lower troposphere, where the wind shear was small, the value of the vorticity depended mainly on the curvature of the streamlines; therefore, the cyclonic and the anticyclonic vorticity generally corresponded to the regions of the troughs and the ridges respectively.

Since both the wind speed and shear increased with height, the value of the vorticity also increased. Thus, maximum value at 500 mb reached $10\text{x}10^{-5}$ sec^{-1}. On the 500-mb surface, as shown in Fig. 7, two vortices were seen; one near the west coast was associated with the cut-off low, and the other over the southeastern United States was associated with the trough.

In the upper troposphere, as seen in Fig. 8, the cyclonic vorticity associated with the western cut-off low attained a value of approximately $20\text{x}10^{-5}$ sec^{-1}, while the value of cyclonic vorticity associated with the eastern cut-off low was $12\text{x}10^{-5}$ sec^{-1}. The maximum anticyclonic vorticity found in the region south of the jet stream was approximately $8\text{x}10^{-5}$ sec^{-1}. This value, although large, was not sufficient to yield a negative absolute vorticity. Due to the decrease of both wind shear and curvature with height above 200 mb, the value of the vorticity at 100 mb was considerably less, namely about $3\text{x}10^{-5}$ sec^{-1}.

If the so called tilting terms are neglected, the vorticity equation becomes

$$\frac{\partial}{\partial t}(q+f)+\mathbf{V}\cdot\nabla(q+f)+\omega\frac{\partial}{\partial p}(q+f)=-(q+f)\nabla\cdot\mathbf{V}$$

and the third term on the left side vanished on the pressure surface of maximum vorticity. Therefore, the divergence on this surface is written as

$$\nabla\cdot\mathbf{V}=-\frac{1}{q+f}\left\{\frac{\partial}{\partial t}(q+f)+\mathbf{V}\cdot\nabla(q+f)\right\} .$$

In this case, the vorticity pattern did not intensify during the period of interest, and the motion of the systems was very slow. Consequently, the contribution of the advection term to the divergence was greater than the contribution of the local time change. In addition, absolute vorticity was positive everywhere. Therefore, at the surface of maximum vorticity, which was between 300 and 200 mb, the areas of positive and negative vorticity advection corresponded to the areas of divergence and convergence respectively. This relation was validated, especially in the vicinity of the cut-off low and the jet stream, at the 200- and the 300-mb surface as seen by comparing Figs. 3, 5, and 8.

IV. TIROS Photographic Observation and Cloud Distribution

The three orbits of TIROS III, 966, 967, and 968, crossed over the United States on Sept. 17, 1961 (Fig. 9). Each orbit contained 32 frames of photographs taken at 30 second intervals. Some of the rectified photographs are shown in Figs. 10, 11, and 12. A composite cloud map made by using these photographs is shown in Fig. 13. Dense clouds are indicated by heavy shadow and thin clouds by stippled areas. The cloud observations from the ground at 1800 GMT, Sept. 17, appear in Fig. 14 for comparison. The correspondence between these two maps is evident, except for the areas in which the nadir angle of the clouds was very large.

The main distinguishable feature in the cloud pattern was a dense cloud band along the east coast, corresponding to the front and the jet stream. As seen in the figure, both northern and southern edges of the band were rather sharp, and so called jet-stream clouds were found to the north of this band. Another dense cloud mass was seen over a small tropical cyclone over the south Atlantic at about 26N and 67W; the fine structure of the clouds could not be seen, since the clouds appeared as a large uniform mass on the photograph. On the Atlantic, between the frontal zone and the tropical cyclone, there were many small cells of the cloud, which were assumed to be some type of cumulus.

Over the Caribbean Sea relatively dense clouds were observed only over islands while there were only scattered clouds over the sea. It is assumed, therefore, that the area under discussion was characterized by a stable low level atmosphere. The

satellite photographs were taken during the mid-afternoon when these tropical islands were expected to be hot. These islands were capable of initiating thermal convection.

In the vicinity of the eastern upper trough, an obscure vortex-shaped cloud pattern was seen. In the Great Lakes area, north of the jet stream, the lakes appeared clearly on the photograph, while thin clouds existed only over the land area. The central part of the United States was almost entirely clear. Although the western parts of the United States and Mexico were covered by rather dense clouds, the distribution of the clouds, especially along the coast, seemed to depend largely on the topographic features. The boundaries of these clouds were not distinct.

It was almost clear over the southern Pacific except for a cloudy area corresponding to the occluded front. In spite of the existence of an axis of rather strong winds in the upper level, neither a jet cloud nor a sharp edge of a cloud band was seen in this area. Therefore, it was supposed that there were some differences in character between this and the eastern cloud zone. To the north of the western cut-off low, dense clouds appeared; however, details of the cloud pattern could not be seen because of the large distance from the satellite.

For comparison between the cloud and the moisture distribution, the dew-point depressions at 500 mb and 700 mb are shown in Fig. 15. The cloud areas generally correspond to those areas in which the dew-point depression is below 10C. There exist two moist zones in the studied area. One is located in the south, extending from the eastern front to the western occluded front through the Gulf and Mexico. The other is in the northern region approximately along the northern wind axis.

Although the correspondence between clouds and divergence patterns was seen generally, there was some discord between these distributions. Examples of this were a cloud area over a divergence area in low levels and a dry area over a convergence area in the low levels. This may have depended partly on the error in the divergence computation, and also may have depended on the fact that cloudiness does not only depend on the vertical motion at a particular moment, but also on the duration of the upward motion for a certain period.

V. The Structure of Fronts and Jet Streams

A number of vertical cross sections were constructed to describe the vertical structure of the front and jet stream. Of these the ones extending from 30N, 70W to 45N, 95W and from 32N, 102W to 55N, 90W are shown in Figs. 16 and 17. The thermal gradient, which yielded the strong wind in the upper troposphere, exists in two frontal zones, partly in the front in the lower troposphere, and mainly in the so called jet front in the higher level.

The potential temperature of the lower boundary of the jet front was about 330K; the potential temperature of the northern extension of the lower boundary was about 340K for the eastern jet stream. Along the cross section for the western United States two wind maxima were observed; both were associated with jet fronts. The potential temperature of the northern jet front was about 340K, and that of the tropopause over the southern wind axis was about 390K. It is known that the potential temperatures of the polar and tropical tropopauses are about 340K and 380K in autumn. Wind speed increased rapidly with height above the lower boundary of the jet front. The maximum wind existed between the upper boundary of the jet front and the tropopause.

With regard to the moisture distribution, as mentioned in the previous section, the areas of small dew-point depression in the middle troposphere were observed in the south side of the wind axes. Just below the maximum wind level the moist zone was found along the south side of the jet axis in the entrance region of the eastern jet stream. Although there existed an entrance of the jet stream to the southeast of the western cut-off low, neither the jet cloud nor the moist area in high levels was evident.

The maximum wind speeds of the western and the eastern jet streams were 100 and 120 knots respectively. The vertical variation of vertical wind shear was about 0.5×10^{-7} cm^{-1} sec^{-1} for both jet streams. The main differences between the two jet streams were the length of the entrance, the curvature of the flow, and the strength of the confluence.

Concerning the western jet, the length of the entrance was short, curvature was anticyclonic, and the confluence was not strong. On the other hand, for the eastern jet stream the length of the entrance region was long, curvature was cyclonic, and the confluence was typical. Some of the features may have had some relation to

the vertical circulation around jet streams. However, no generalizations could be made from this case study.

The cloud band along the eastern front, as seen on the cloud photograph, seemed to have a single structure from its southern edge to its northern edge. However, it should be understood that the clouds associated with the front in the lower troposphere and the jet clouds which existed above the jet front were not a continuous system.

The direction of cloud streets has some relation to the wind direction. By simple calculations it can be shown that the cloud street could be oriented parallel to the wind shear vector, if it is assumed that the cloud moves with the wind at the point where the cloud exists. Two cases are considered to show this possible relation, one without vertical motion and the other with vertical motion.

In the first case, it is assumed that the cloud mass exists in the layer between Z_0 and Z_1, in which no vertical motion exists. It is also assumed that the horizontal wind varies linearly with height. The x axis is taken along the wind on the lower boundary. Let U_0, U_1, and V_1 be the wind components on the levels of Z_0 and Z_1. The wind components at a point in the layer are

$$u = u_0 + \frac{u_1 - u_0}{z_1 - z_0}(z - z_0) \quad \text{and} \quad v = \frac{v_1}{z_1 - z_0}(z - z_0) \quad ;$$

where Z is the height of the point considered. The position of the cloud at the height Z, after the time t, is therefore,

$$x = \left\{ u_0 + \frac{u_1 - u_0}{z_1 - z_0}(z - z_0) \right\} t \quad \text{and} \quad y = \frac{v_1}{z_1 - z_0}(z - z_0)\, t \quad .$$

The projection of the cloud mass onto the horizontal plane is obtained by eliminating t, yielding the result that

$$x = u_0 t + \frac{u_1 - u_0}{v_1} y \quad .$$

This means that the cloud mass appears on the photograph to be stretched parallel to the wind shear vector in the corresponding layer.

Secondly, a case with vertical motion is considered. It is assumed that the horizontal wind varies linearly with height and that the vertical velocity is a function of Z only. With regard to the cloud particle, which begins ascending from the height

Z_0 at the moment $t = \tau$, the relation between Z and t is

$$\int_{Z_0}^{Z} \frac{dZ}{W(Z)} = t - \tau \quad .$$

Therefore, the height of this particle is the function of $t-\tau$;

$$Z = \begin{cases} f(t-\tau) + Z_0 & \text{for } t > \tau \\ Z_0 & \text{for } t \le \tau \end{cases} \quad .$$

The horizontal velocity of this particle at time, t, is

$$u(t,\tau) = \begin{cases} u_0 + \frac{U_1 - U_0}{Z_1 - Z_0} \cdot f(t-\tau) & \text{for } t > \tau \\ u_0 & \text{for } t \le \tau \end{cases}$$

and

$$v(t,\tau) = \begin{cases} \frac{V_1}{Z_1 - Z_0} \cdot f(t-\tau) & \text{for } t > \tau \\ 0 & \text{for } t \le \tau \end{cases} \quad .$$

The position of this particle at time, t, is obtained by integrating the velocity with respect to time, yielding

$$x(t,\tau) = u_0 t + \frac{U_1 - U_0}{Z_1 - Z_0} \cdot \int_{\tau}^{t} f(t-\tau)\, dt$$

and

$$y(t,\tau) = \frac{V_1}{Z_1 - Z_0} \cdot \int_{\tau}^{t} f(t-\tau)\, dt \quad .$$

As in the first case, the projection of the cloud mass onto the horizontal plane is obtained by the elimination of τ. This calculation yields

$$x = u_0 t + \frac{U_1 - U_0}{V_1} y \quad .$$

The projection of the cloud onto the horizontal plane is again parallel to the wind shear vector.

The assumptions used above are an oversimplification, because the cloud does not move with the flow, but may change in other processes; also wind and vertical motion may change with time. Therefore, the above mentioned result should be considered as a rough approximation.

It also should be mentioned that the elongated cloud pattern on the photograph is not along a streamline or a trajectory, but is the projection of a cloud mass which

exists in the same layer onto a horizontal plane. Therefore, physically, the orientation of the cloud street must be due to winds in a layer rather than the winds at a surface.

The direction of the geostrophic wind shear is that of the thermal wind. The thickness charts for the layers bounded by 700 and 500 mb, and 500 and 300 mb are shown in Fig. 18. The orientation of the jet clouds associated with the eastern jet stream is parallel to the thickness lines for the layer between 500 and 300 mb. Also the orientation of the clouds in the vicinity of the eastern cut-off low is approximately parallel to these thickness lines. These facts are considered to be a validation for the above mentioned relations.

VI. The Distributions of Tropopause and Maximum Wind

The distributions of the tropopause height, measured in pressure, i. e., in mb, and the potential temperatures of the tropopause are shown in Fig. 19. A strong gradient of both tropopause height and potential temperature, called a tropopause break line, is observed approximately at 40N. The variation of the tropopause height is very remarkable within the break zone and very small on either side of this zone. The potential temperature of the tropopause along the break line is about 350K, and those in the northern and the southern regions are about 330K and 370K respectively. The mean potential temperatures of the tropical and the polar tropopauses in autumn are known to be 370K and 340K.

Over the western cut-off low the height of the tropopause was remarkably low, namely about 300 mb; also the potential temperature at the tropopause was very low, namely about 320K. This was a typical feature of the deep cut-off low. Over the eastern cut-off low, however, these features were not distinguishable.

The distributions of maximum wind speed and the height of the maximum wind level measured in units of pressure are shown in Fig. 20. As seen in Fig. 20, two axes of wind maxima are evident. One is located along the northern edge of the subtropical highs in the upper troposphere, the other along the tropopause break line in the north side. Two flows form typical confluence patterns in front of the cut-

off lows. With regard to the height of the maximum wind level, the zones of low height exist along the axes of maximum wind. The height of the maximum wind is especially low around the western cut-off low, namely below 350 mb. The area of high maximum wind level, which coincided with the area of weak wind, is seen over the central United States between the two cut-off lows.

VII. Summary and Conclusions

This study considers only one synoptic case of jet streams. However, the results do not seriously disagree with past research. Therefore, it is assumed that the case presented in this study is representative of the general case of jet streams.

The main results of this investigation are as follows:

A jet stream exists between the tropopause and the jet front in the upper troposphere. The horizontal thermal gradient, which yields jet streams, exists mainly in the jet front rather than in the front in the lower troposphere during summer.

The moist and cloudy areas in the middle troposphere are to the south of jet streams in the entrance and neutral regions. The jet cloud is found in the entrance region of strong jets just to the south of the wind core. A jet cloud and the cloud which is associated with the front in the lower troposphere are another system even though they appear to be a single cloud mass on the photograph. The direction of these jet clouds is approximately along the direction of the thermal wind or geostrophic wind shear in the corresponding layer.

In this study rectified TIROS photographs were used to determine the precise location of jet-stream nephsystems. Without the data obtained from these satellite photographs a major portion of this study could not be completed. Therefore, it is concluded that, in the absence of other data, satellite photographs are an indispensable aid to both research in jet-stream clouds and operational forecasting.

Acknowledgements

The author's synoptic and photogrammetric works were performed in the Mesometeorology Project, Department of Geophysical Sciences, the University of Chicago.

The author is grateful to acknowledge Dr. Tetsuya Fujita for his kind guidance and stimulating discussions. Sincere gratitude should be expressed to the staff members of the Mesometeorology Project, especially Mr. Joseph Goldman, for their assistance in the completion of this paper.

References

Bowley, C. J., et al., 1962: Satellite observations of wake formation beneath an inversion. J. Atmos. Sci., 19, 52-55.

Conover, J. H., 1960: Cirrus patterns and related air motion near the jet stream as derived by photography. J. Meteor., 17, 270-282.

Defant, F., and H. Taba, 1958: The break down of zonal circulation during the period Jan 8 to 13, 1956, the characteristic of temperature field and tropopause and its relation to atmospheric field of motion. Tellus 10, 430-450.

Endlich, R. M., and G. S. McLean, 1957: The structure of the jet stream core. J. Meteor., 14, 543-552.

Fujita, T., 1961: Outline of a technique for precise rectification of satellite cloud photographs. Res. Paper 3, Mesomet. Proj., U. of Chicago.

Kochansky, A., 1955: Cross sections of the mean zonal flow and temperature along 80W. J. Meteor., 12, 95-106.

Krueger, A. F., and S. Fritz, 1961: Cellular cloud patterns revealed by TIROS I. Tellus 13, 1-7.

Kuettner, J., 1959: The band structure of the atmosphere. Tellus 11, 267-294.

McLean, G. S., 1957: Cloud distribution in the vicinity of jet stream. Bull. Amer. Meteor. Soc., 38, 579-583.

Mohri, K., 1957: Jet streams and upper fronts in general circulation and their characteristics over the Far East. Geophys. Mag., 29, 45-125 (part I), 333-412 (part II).

Reiter, E. R., 1957: The layer of maximum wind. J. Meteor., 15, 27-43.

Riehl, H., et al., 1954: The jet stream. Meteorol. Monographs, Vol. 2, No. 7.

Schaefer, V. J., 1953: Cloud forms of the jet stream. Tellus 5, 27-31.

----------, and W. E. Hubert, 1955: A case study of jet stream clouds. Tellus 7, 301-307.

Taba, H., 1959: The horizontal and vertical wind profiles of the subtropical and polar jet for Jan 1-7, 1959, and the variation of the equivalent barotropic level. Tellus 11, 441-451.

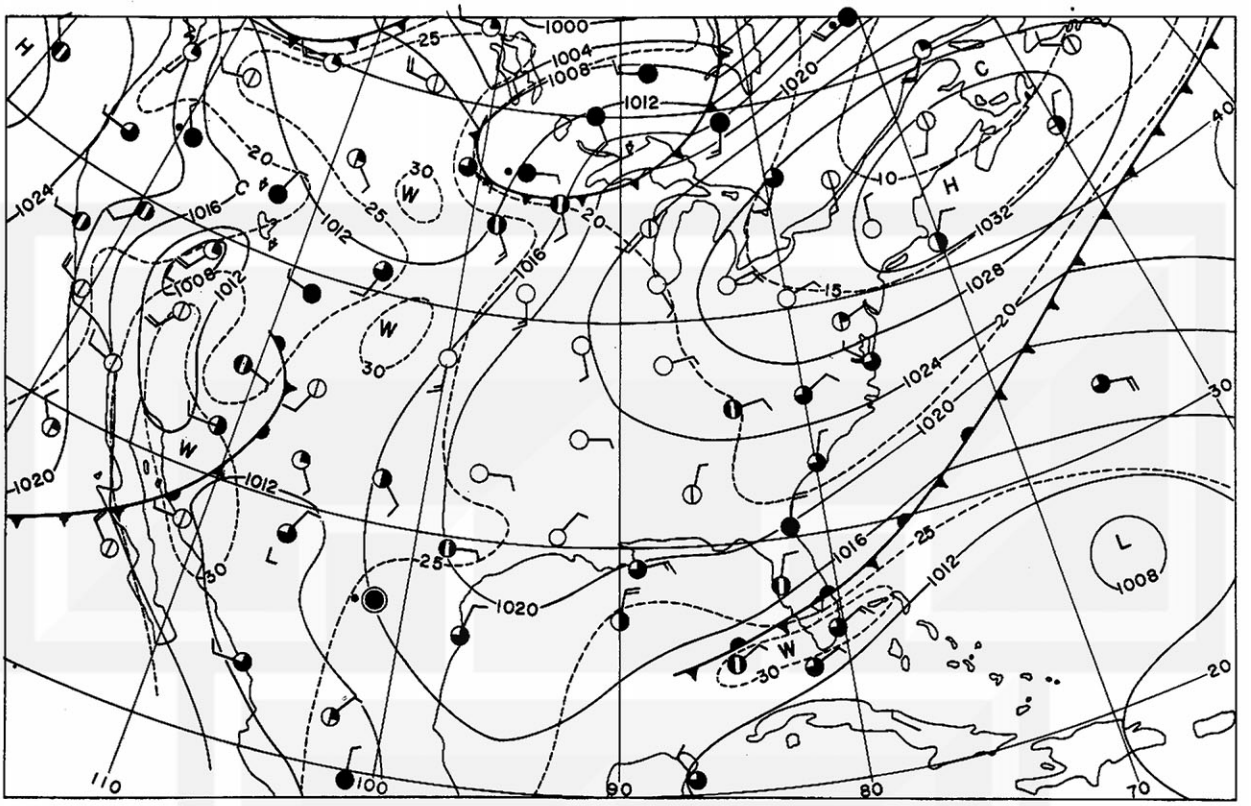

Fig. 1. Surface chart for 0000 GMT, Sept. 18, 1961. Isobars (continuous lines) and isotherms (dashed lines) are drawn at every 4 mb and 5C, respectively.

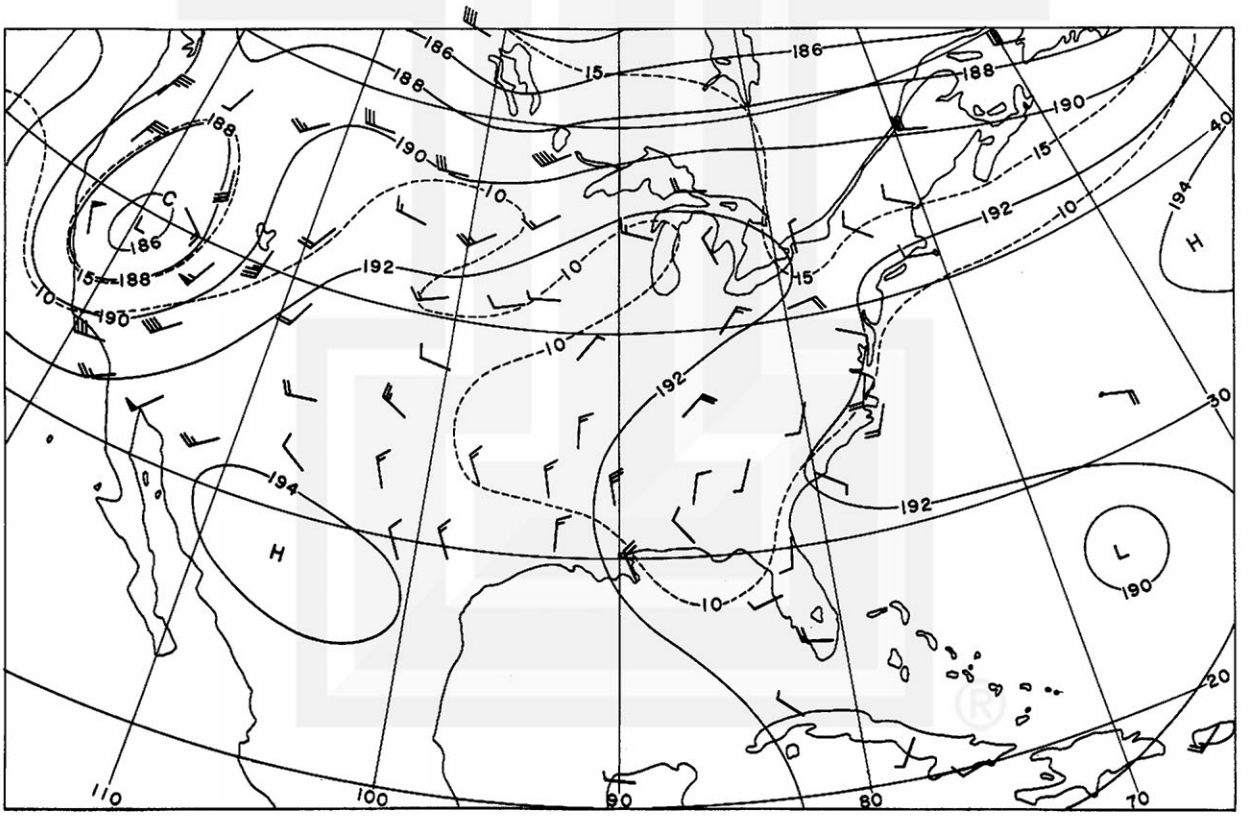

Fig. 2. 500-mb chart for 0000 GMT, Sept. 18, 1961. Height contours (continuous lines) and isotherms (dashed lines) at every 200 gpft and 5C.

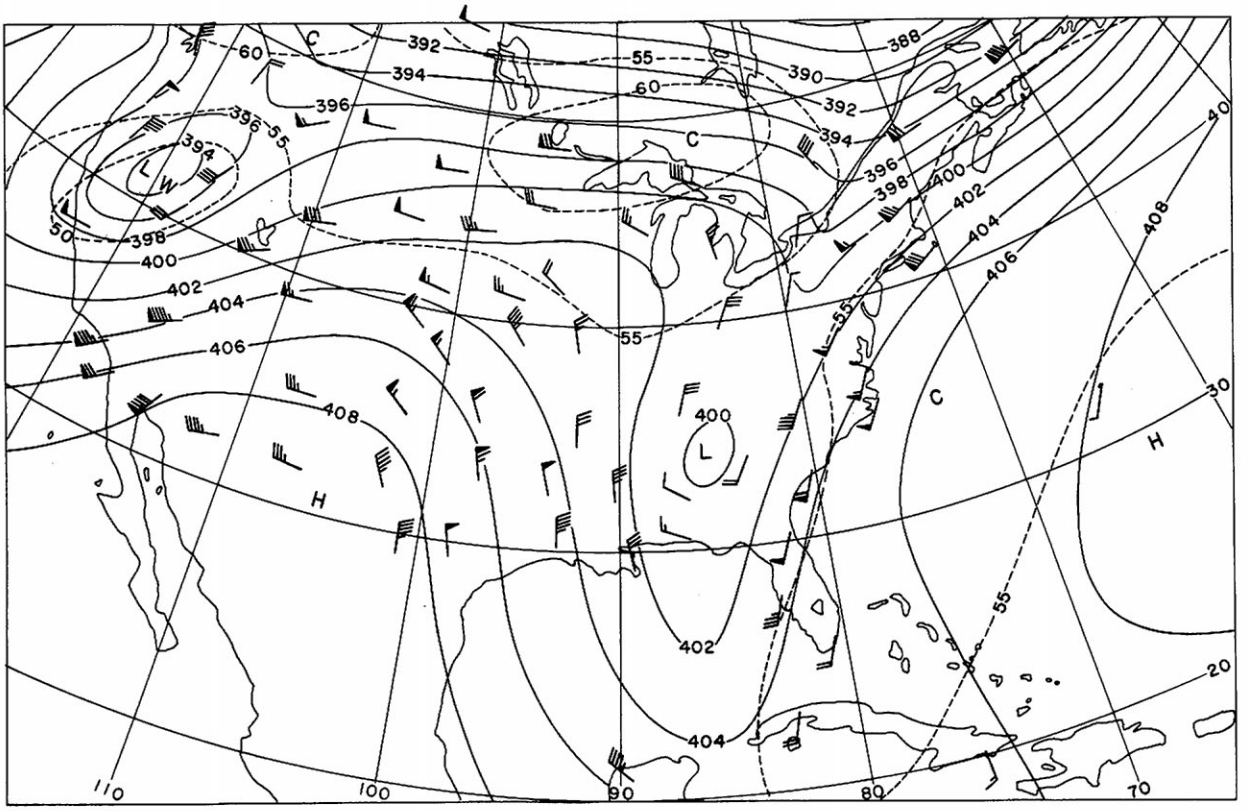

Fig. 3. 200-mb chart for 0000 GMT, Sept. 18, 1961. Height contours (continuous lines) and isotherms (dashed lines) at every 200 gpft and 5C.

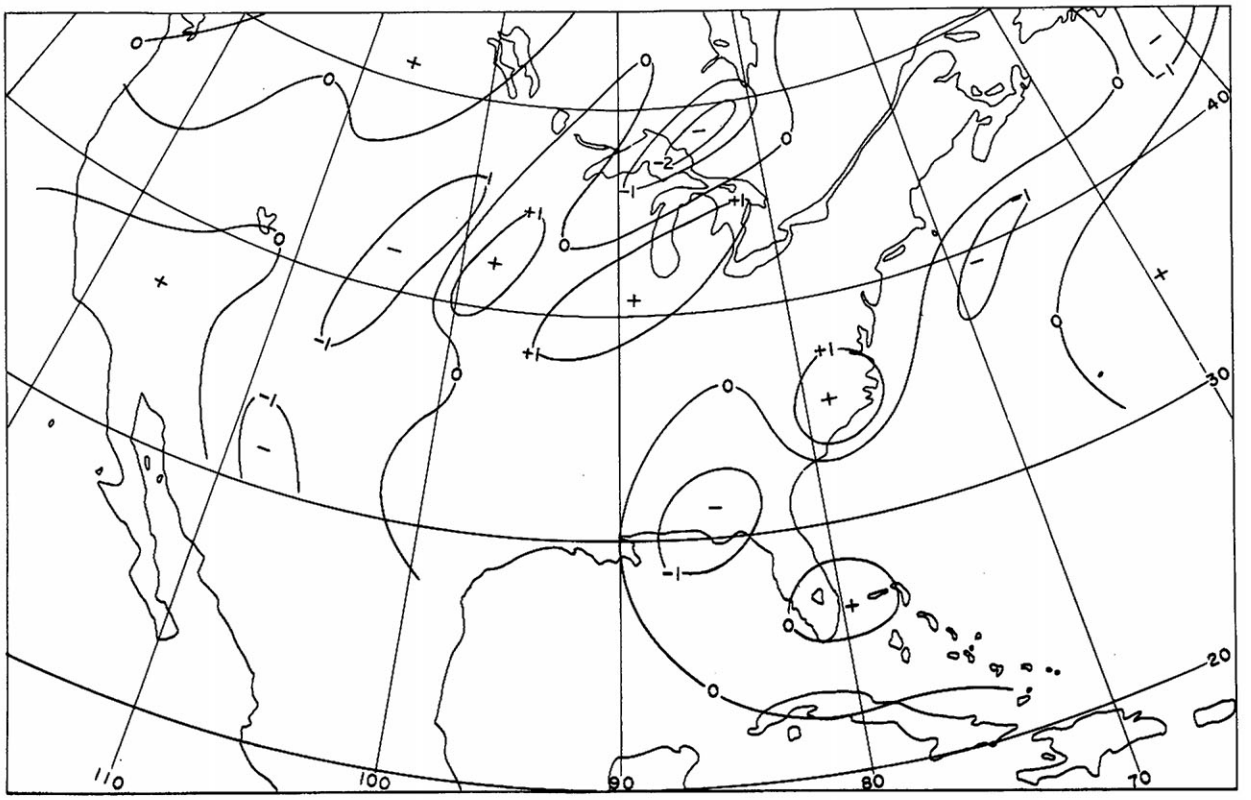

Fig. 4. Divergence at 850 mb for 0000 GMT, Sept. 18, 1961. Unite in 10^{-5} sec^{-1}.

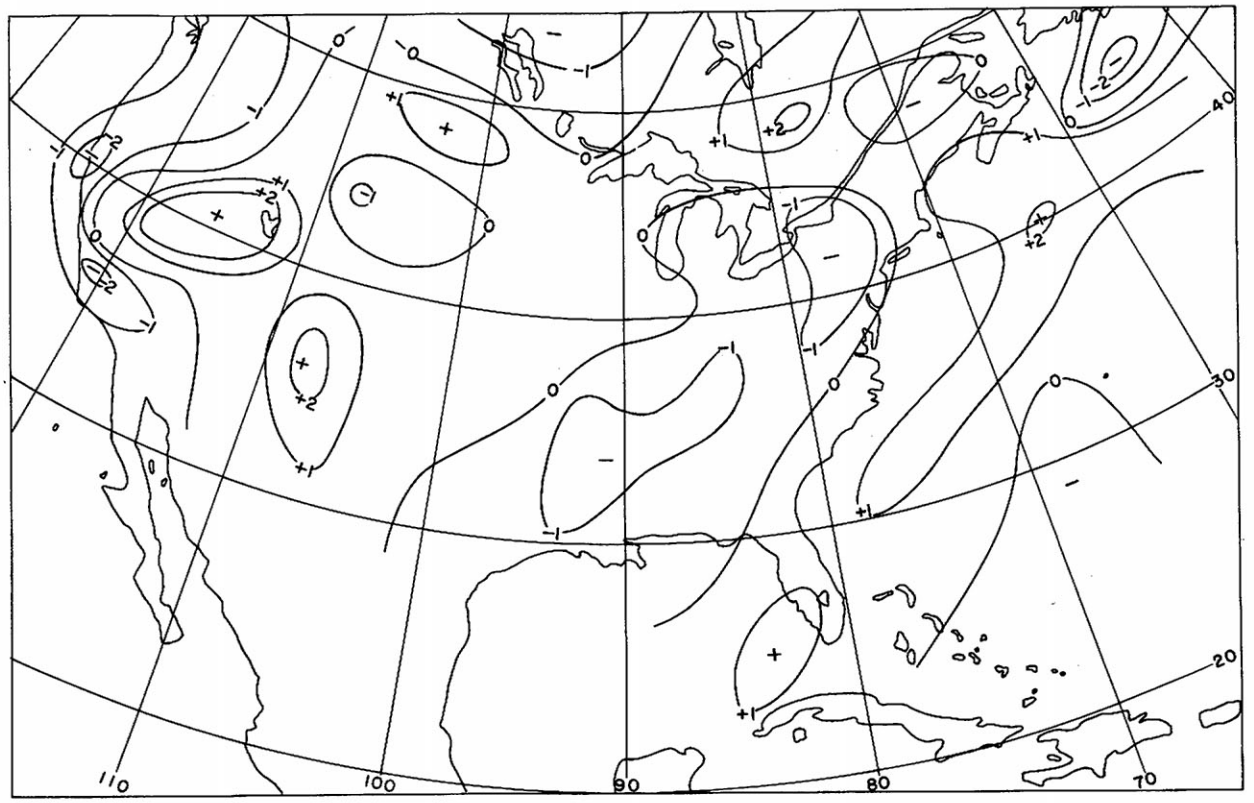

Fig. 5. Divergence at 300 mb for 0000 GMT, Sept., 1961. Unite in 10^{-5} sec^{-1}.

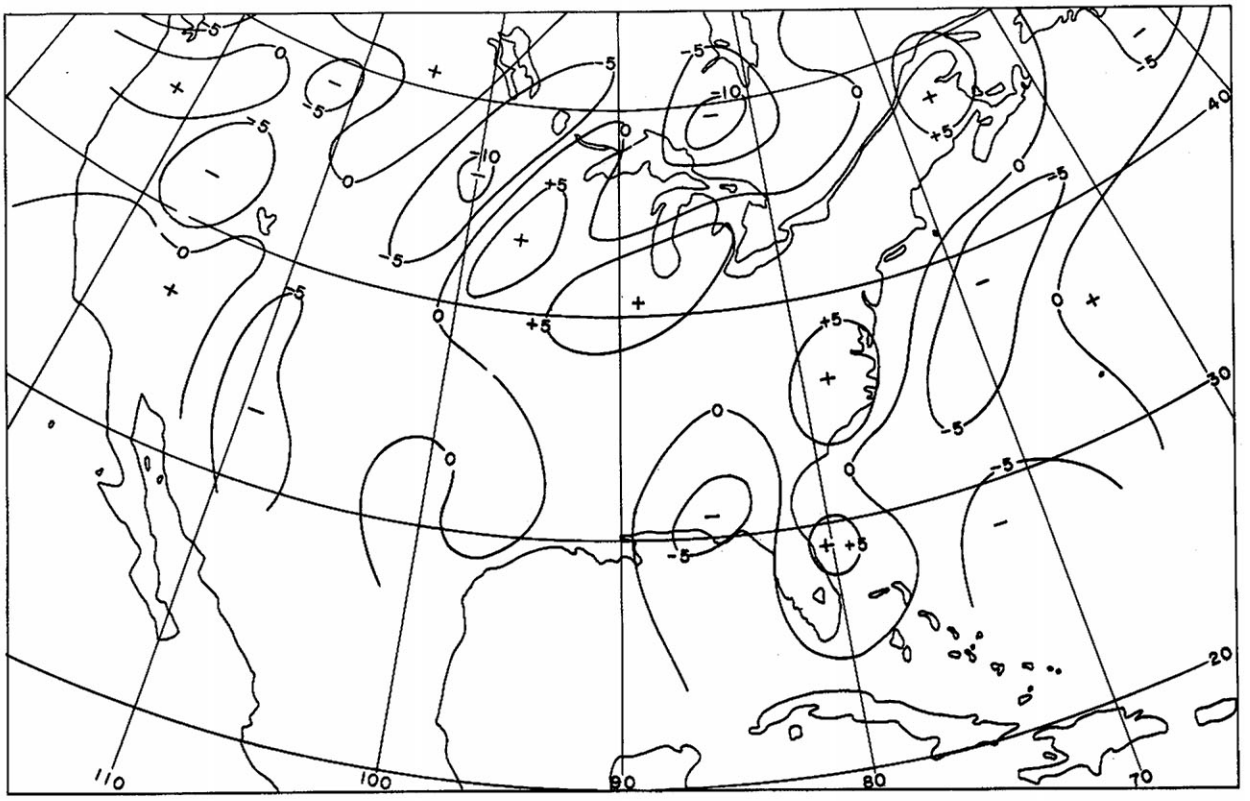

Fig. 6. Mean value of divergence at 850 mb and 700 mb for 0000 GMT, Sept. 18, 1961. Unite in 10^{-6} sec^{-1}.

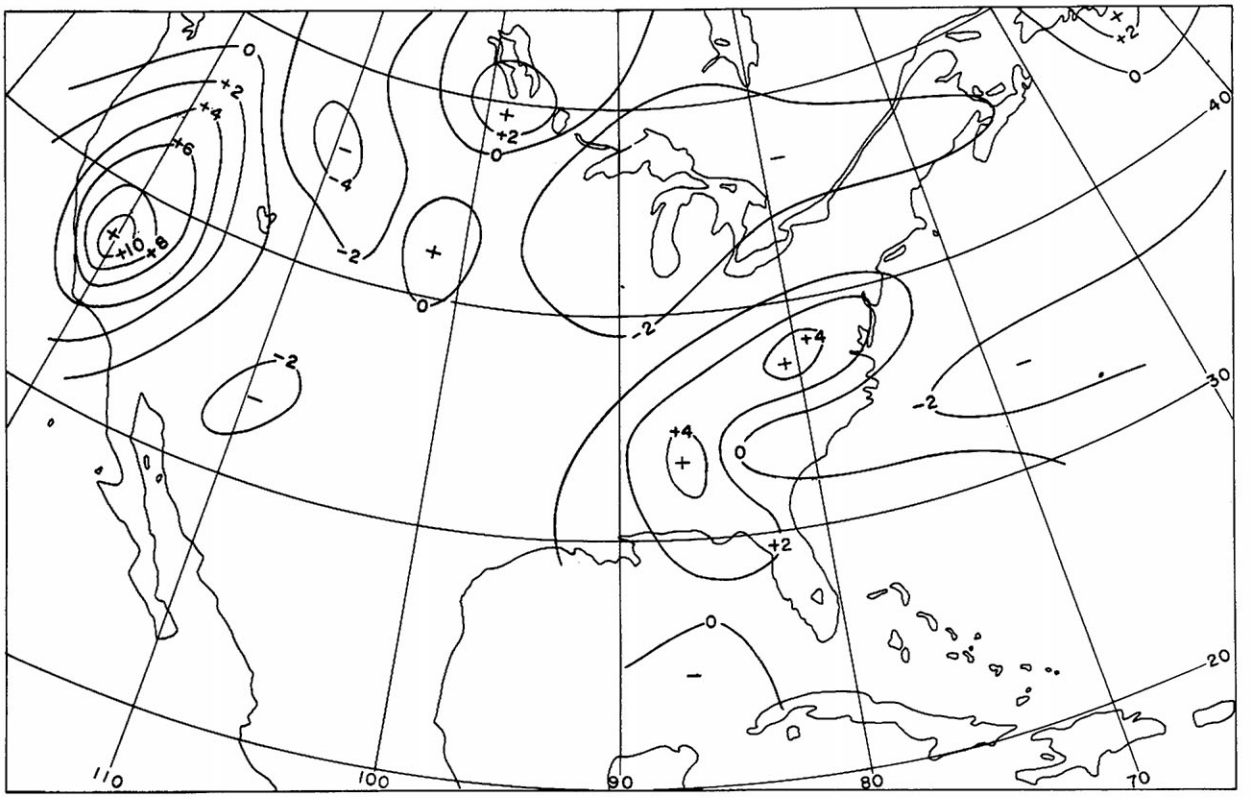

Fig. 7. Vorticity at 500 mb for 0000 GMT, Sept. 18, 1961. Unite in 10^{-5} sec^{-1}.

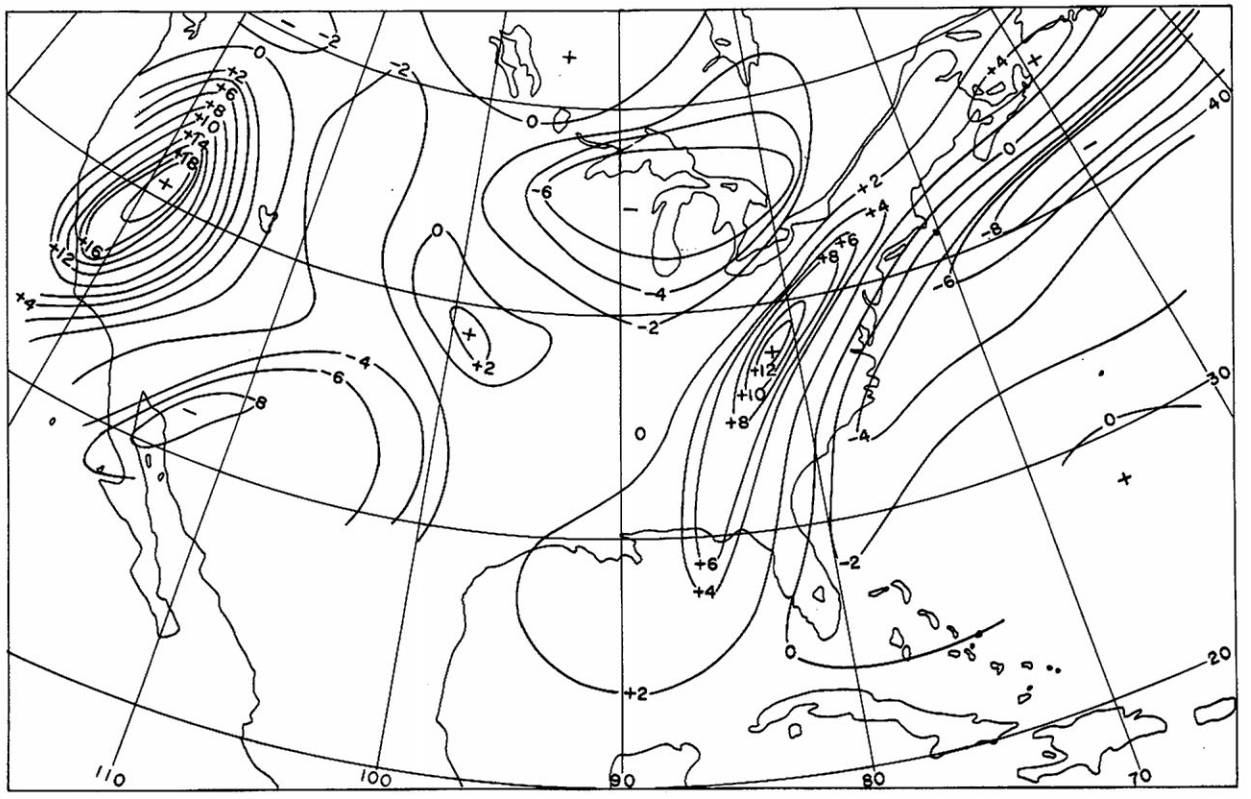

Fig. 8. Vorticity at 300 mb for 0000 GMT, Sept., 18, 1961. Unite in 10^{-5} sec^{-1}.

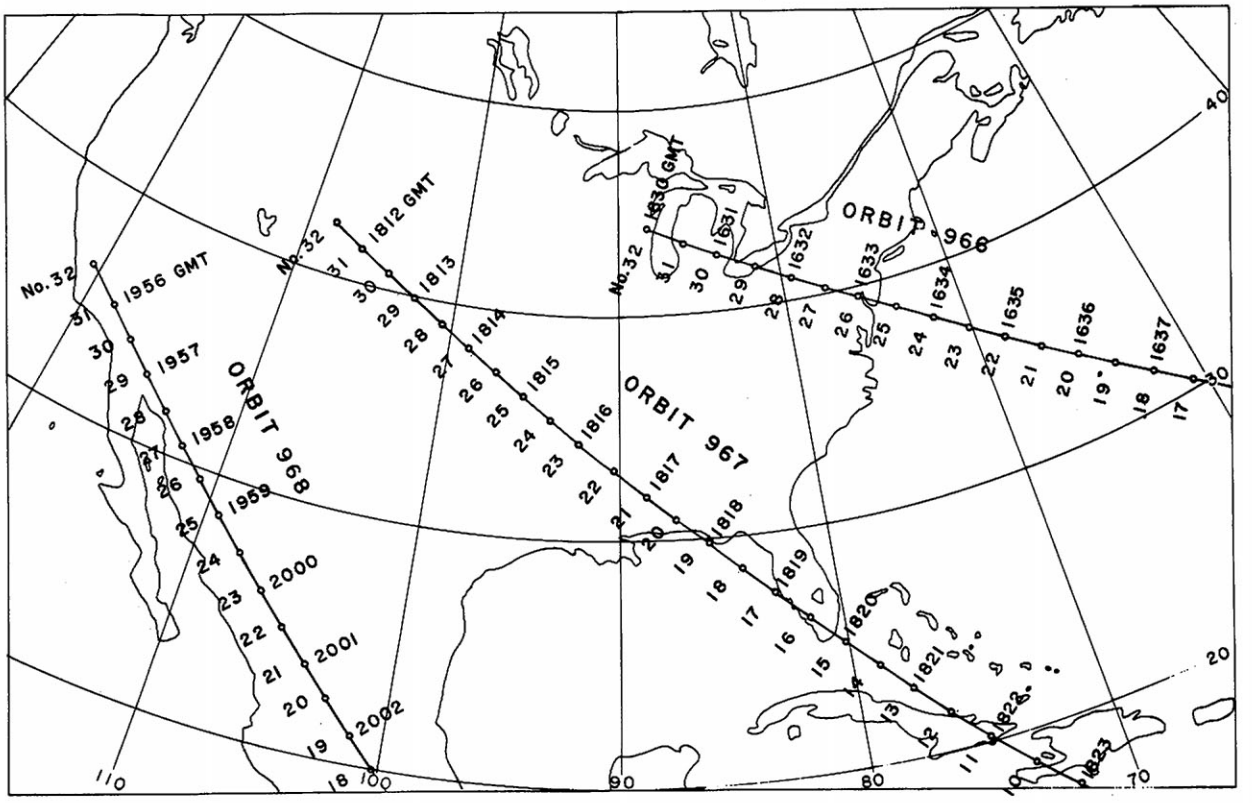

Fig. 9. Terrestrial satellite subpoint (TSP) track of TIROS III, Orbits 966, 967, 968 on Sept. 17, 1961. Numbers entered along the tracks are frame numbers and times.

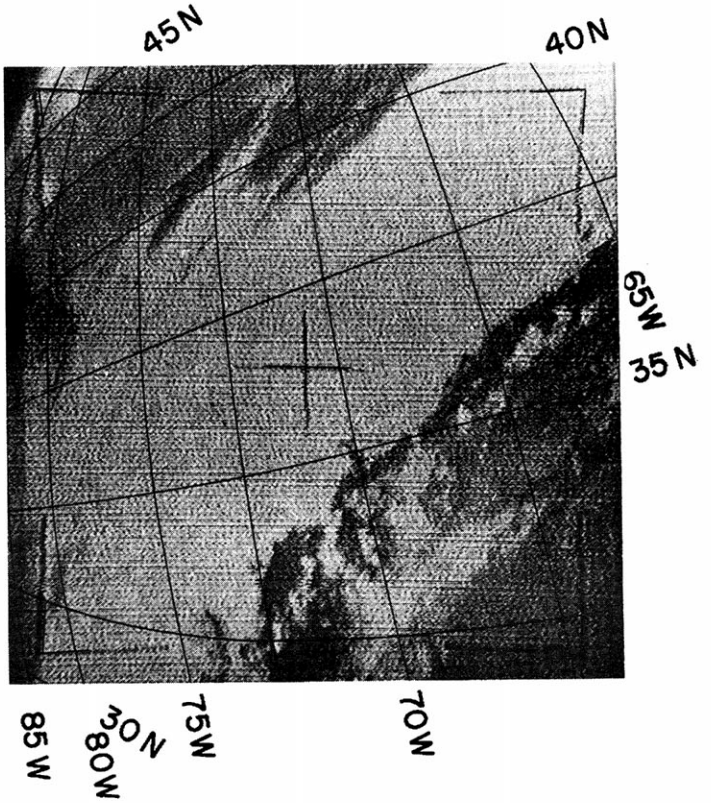

Fig. 10. Rectified TIROS photograph, TIROS III, Orbit 966, Frame No. 21 at $16^{h}35^{m}30^{s}$ GMT, Sept. 17, 1961.

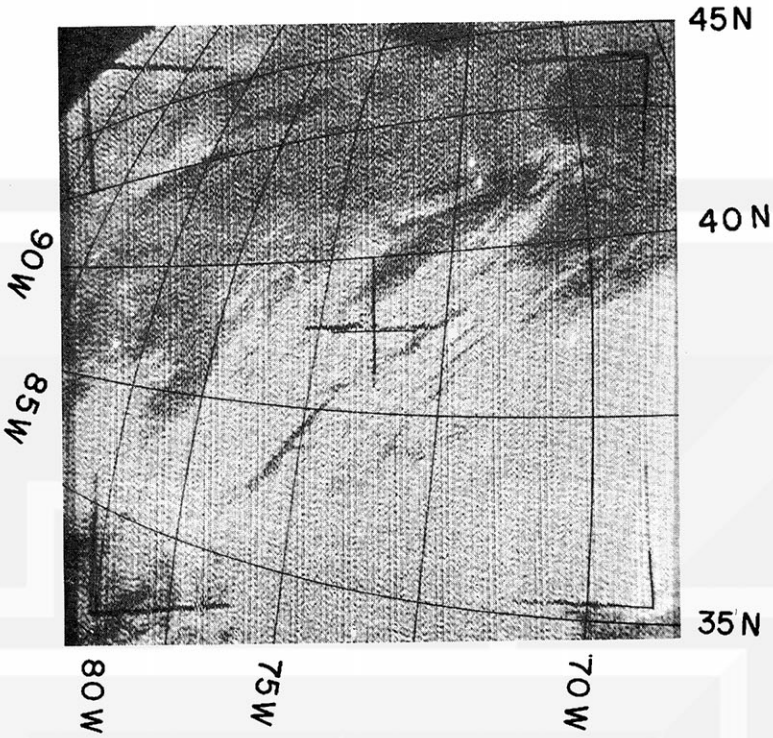

Fig. 11. Rectified TIROS photograph, TIROS III, Orbit 966, Frame No. 23 at $16^h 34^m 30^s$ GMT, Sept. 17, 1961.

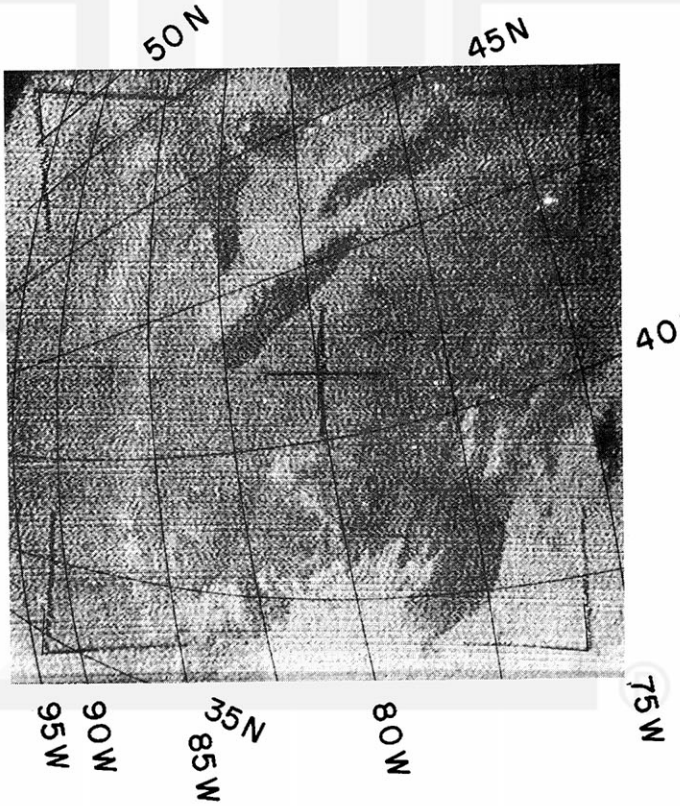

Fig. 12. Rectified TIROS photograph, TIROS III, Orbit 966, Frame No. 26 at $16^h 33^m 00^s$ GMT, Sept. 17, 1961.

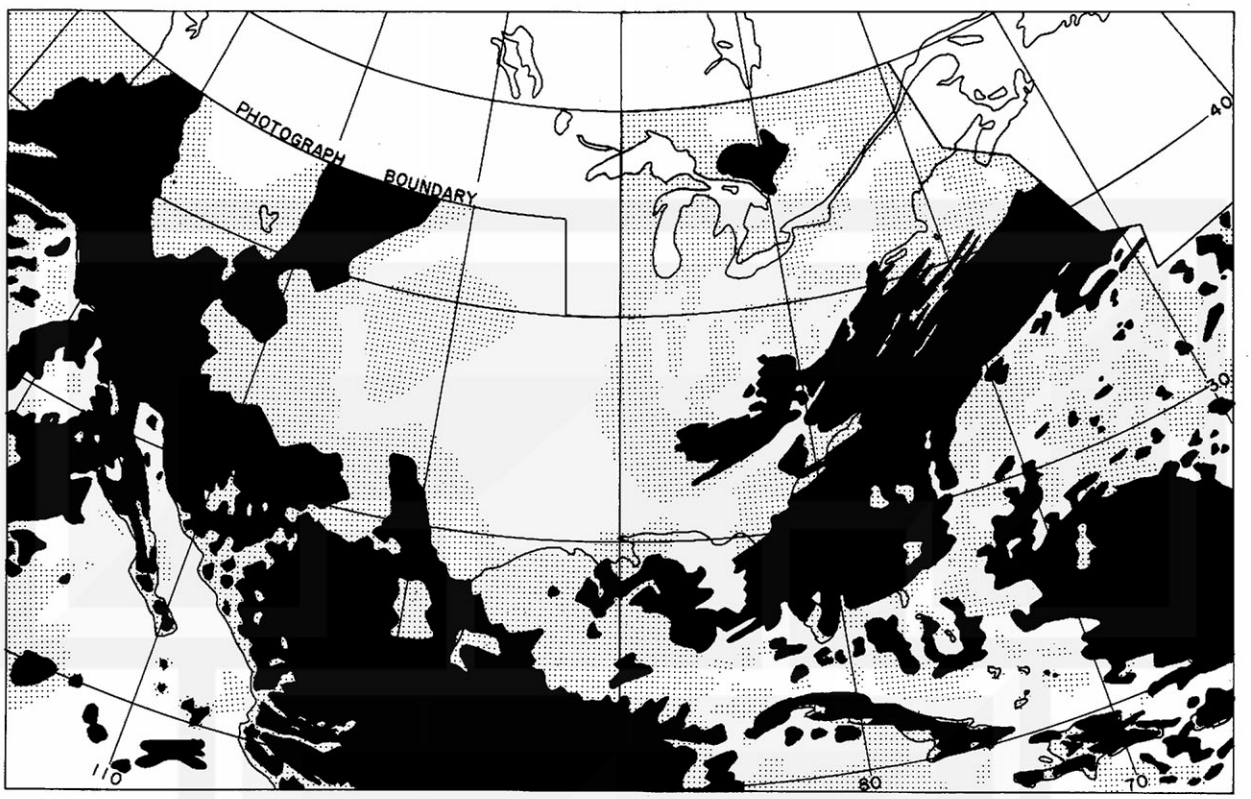

Fig. 13. Composite cloud patterns during 1630-2003 GMT, Sept. 17, 1961.

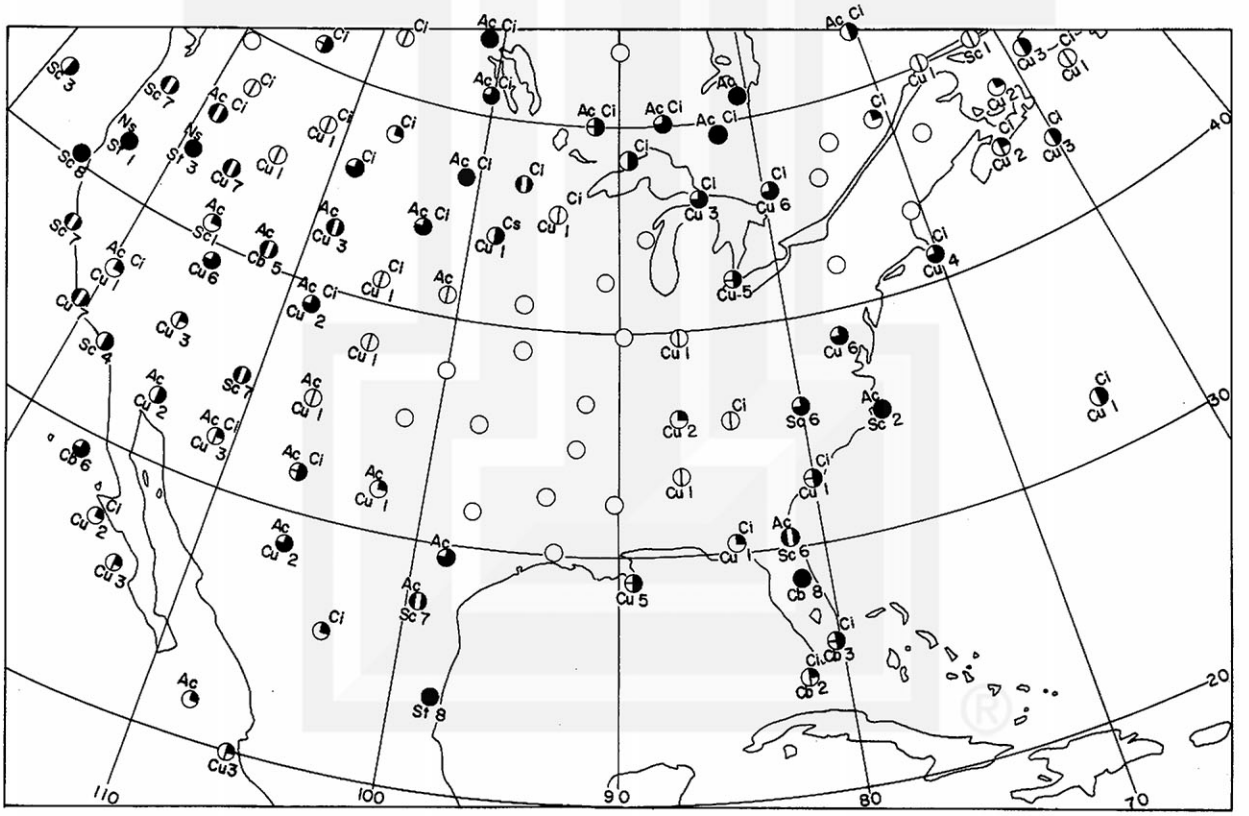

Fig. 14. Cloud observations from ground at 1800 GMT, Sept. 17, 1961. Letters and numbers indicate the cloud type and the lower cloud cover.

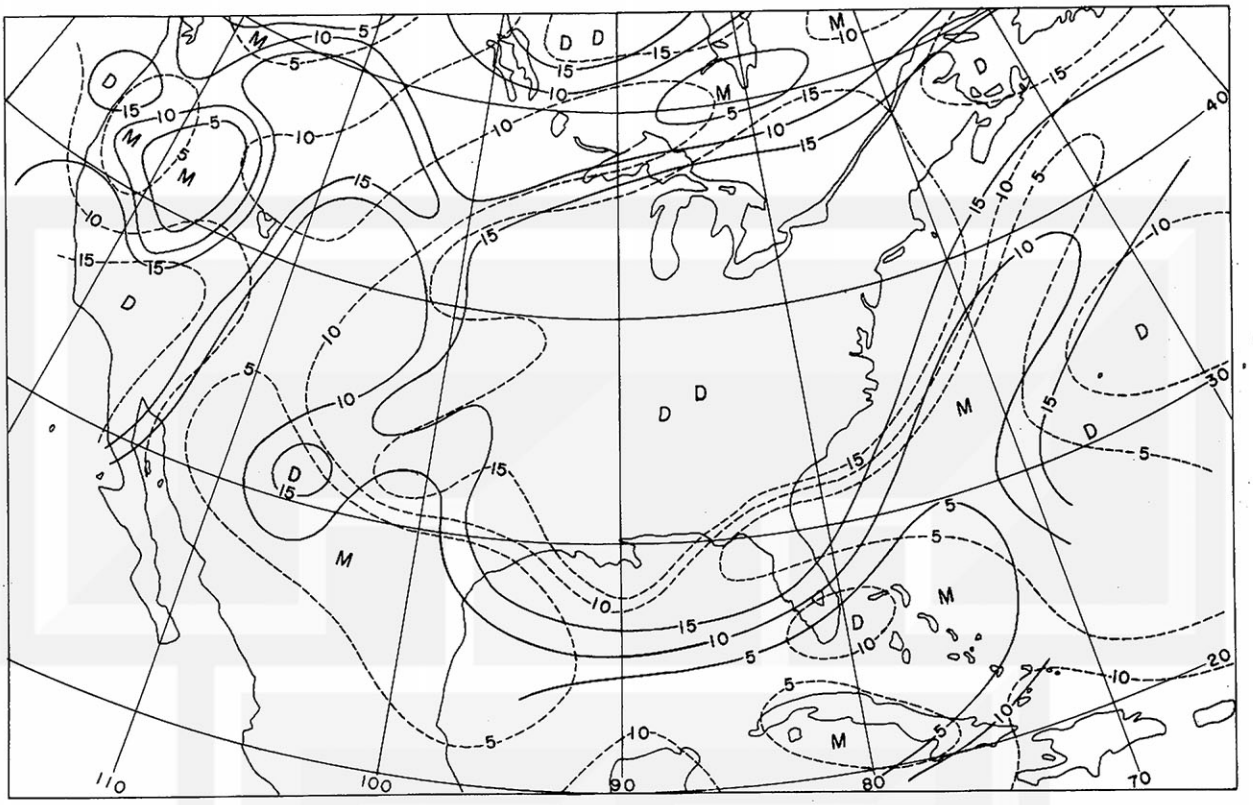

Fig. 15. Dew-point depression at 500 mb (continuous lines) and at 700 mb (dashed lines) for 0000 GMT, Sept. 18, 1961. (slant letters for 700 mb)

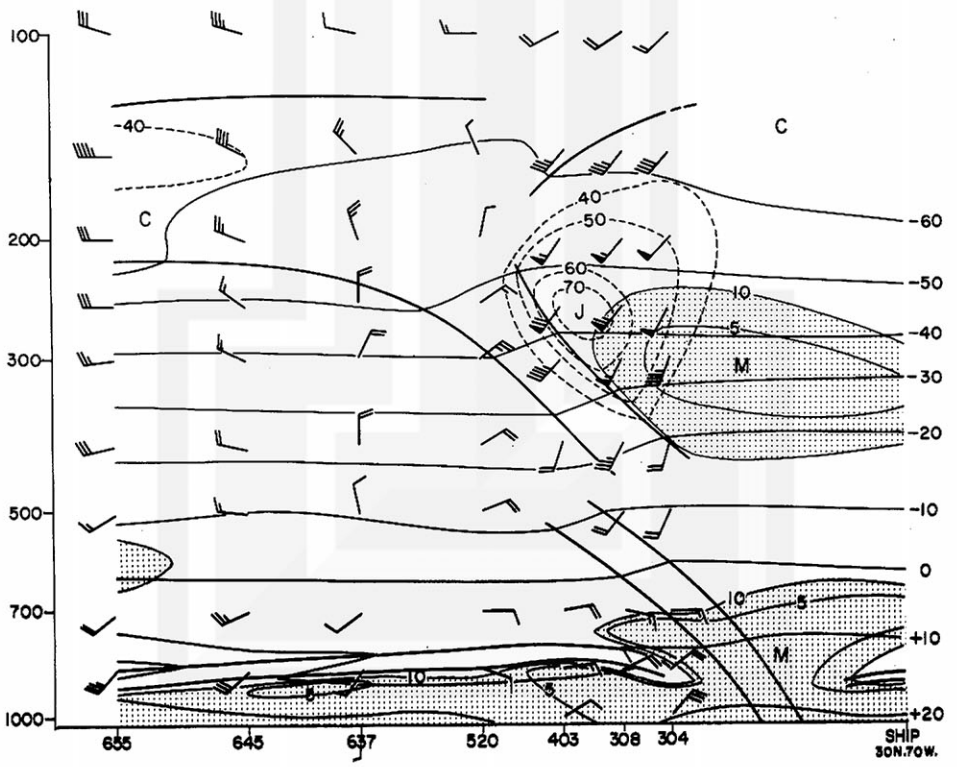

Fig. 16. Vertical cross section from 30N 70W to 45N 95W for 0000 GMT, Sept. 18, 1961. Isotherms (thin continuous lines) and isotachs (dashed lines) at every 10C and 10 knots. Heavy solid lines indicate discontinuous surfaces. Stippled areas indicate moist areas in which dew-point depressions are less than 10C.

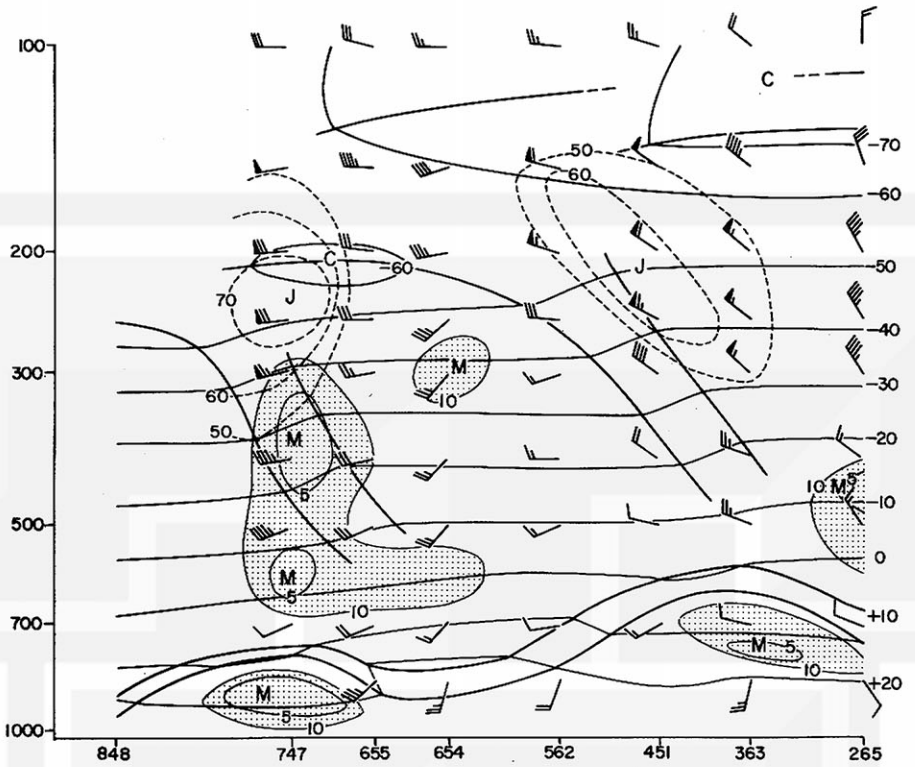

Fig. 17. Vertical cross section from 32N 102W to 55N 90W for 0000 GMT, Sept. 18, 1961.

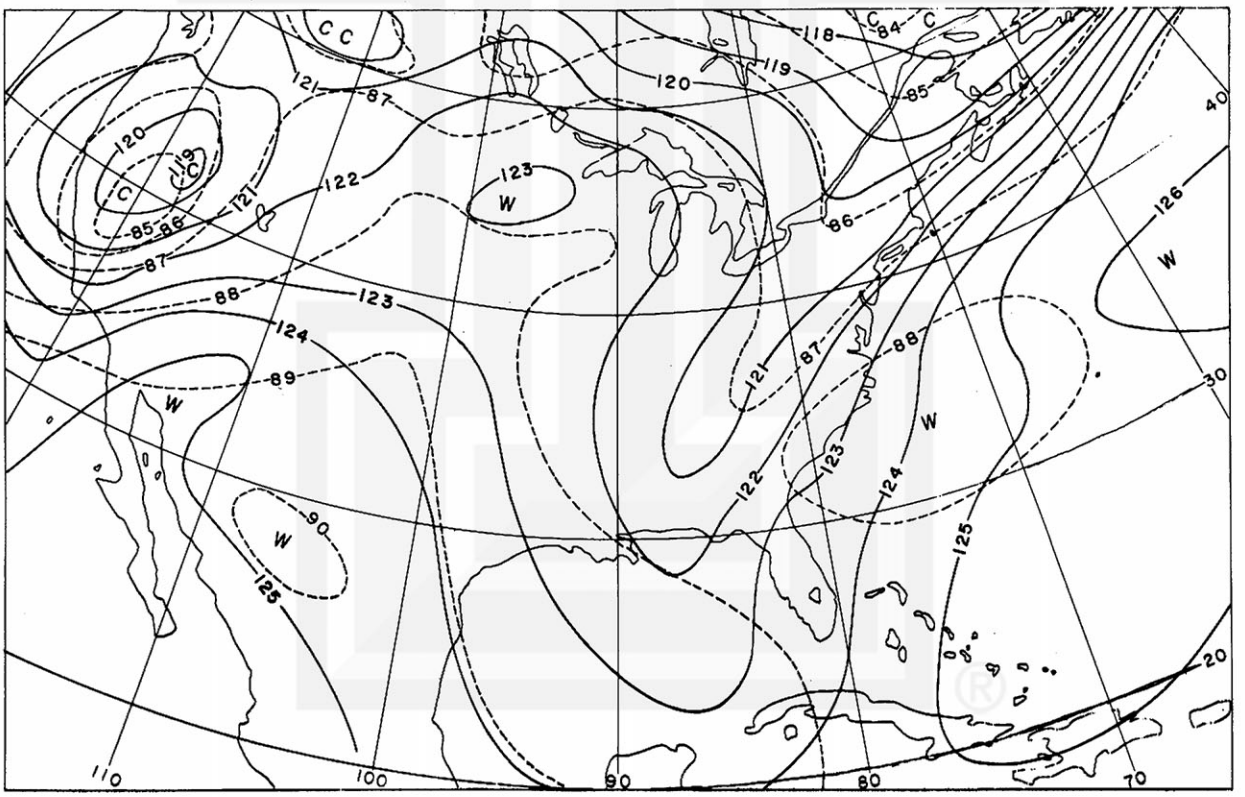

Fig. 18. Thickness chart for 0000 GMT, Sept. 18, 1961. Thickness lines of 300-500 mb (continuous lines) and 500-700 mb (dashed lines) at every 100 gpft. (Slant letters for 500-700 mb)

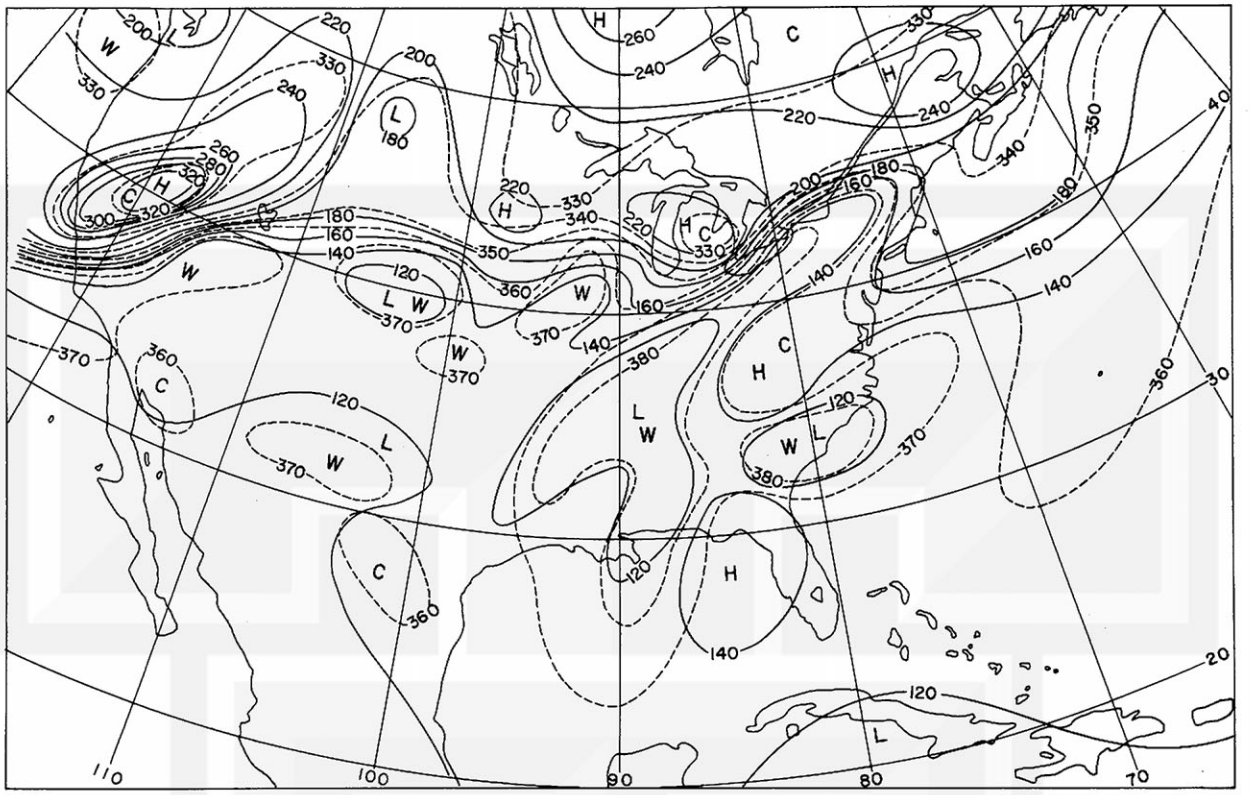

Fig. 19. Tropopause chart for 0000 GMT, Sept. 18, 1961. Pressure of tropopause (continuous lines) and potential temperature on tropopause (dashed line) are in mb and K.

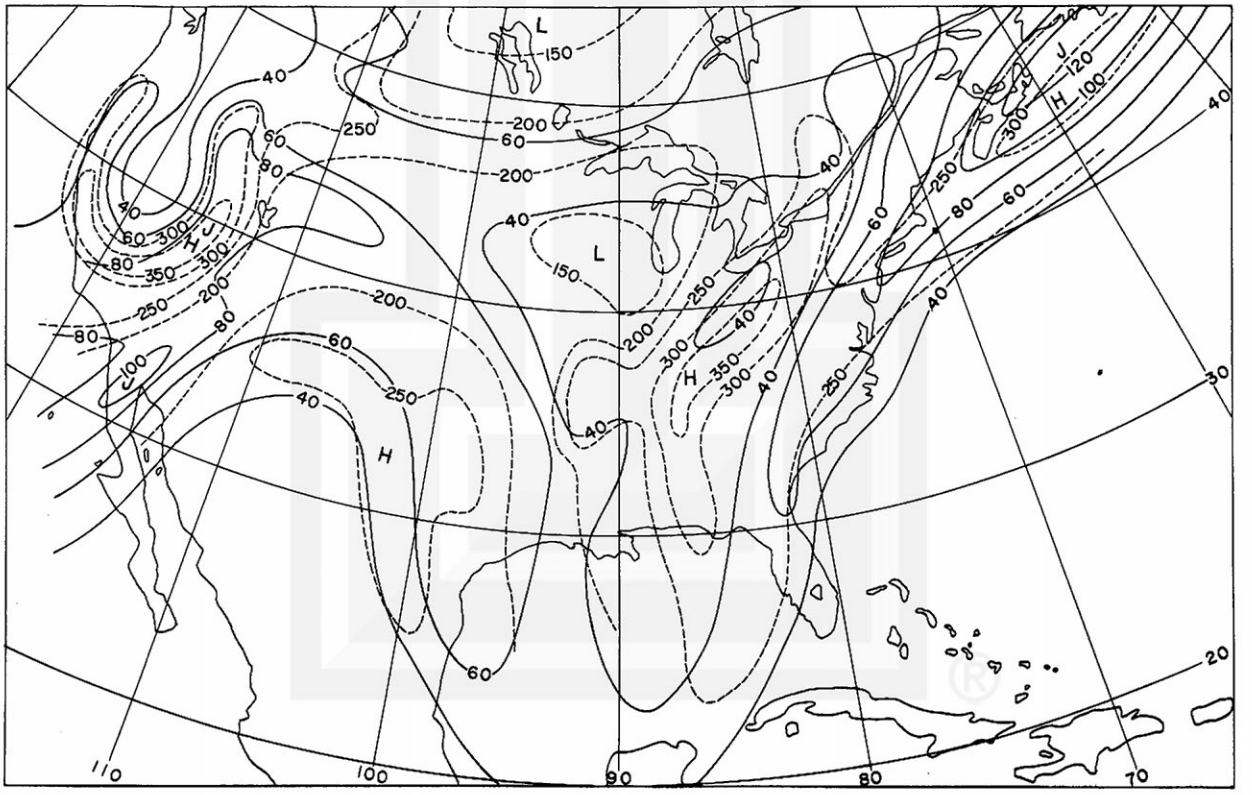

Fig. 20. Maximum wind chart for 0000 GMT, Sept. 18, 1961. Maximum wind speeds (continuous lines) and pressure of maximum wind level (dashed lines) are in knots and mb.

MESOMETEOROLOGY PROJECT ---- RESEARCH PAPERS

1. Report on the Chicago Tornado of March 4, 1961 - Rodger A. Brown and Tetsuya Fujita

2. Index to the NSSP Surface Network - Tetsuya Fujita

3. Outline of a Technique for Precise Rectification of Satellite Cloud Photographs - Tetsuya Fujita

4. Horizontal Structure of Mountain Winds - Henry A. Brown

5. An Investigation of Developmental Processes of the Wake Depression Through Excess Pressure Analysis of Nocturnal Showers - Joseph L. Goldman

6. Precipitation in the 1960 Flagstaff Mesometeorological Network - Kenneth A. Styber

7. On a Method of Single- and Dual-Image Photogrammetry of Panoramic Aerial Photographs - Tetsuya Fujita

8. A Review of Researches on Analytical Mesometeorology - Tetsuya Fujita

9. Meteorological Interpretations of Convective Nephsystems Appearing in TIROS Cloud Photographs - Tetsuya Fujita, Toshimitsu Ushijima, William A. Hass, George T. Dellert, Jr.

10. Study of the Development of Prefrontal Squall-Systems Using NSSP Network Data - Joseph L. Goldman

11. Analysis of Selected Aircraft Data from NSSP Operation, 1962 - Tetsuya Fujita

12. Study of a Long Condensation Trail Photographed by TIROS I - Toshimitsu Ushijima

13. A Technique for Precise Analysis of Satellite Data; Volume I -- Photogrammetry - Tetsuya Fujita